Communication

Multiparameter Modeling With ANN for Antenna Design

Li-Ye Xiao, Wei Shao, Fu-Long Jin, and Bing-Zhong Wang

***Abstract*— In this communication, a novel artificial neural network (ANN) model is proposed to describe the antenna performance with various parameters. In this model, three parallel and independent branches are involved for three different performance parameters. Meanwhile, a data-classification technique of support vector machine is also included to classify geometrical variables into the proper categories. Once the geometrical variables are input, the ANN model can simultaneously obtain S-parameter, gain, and radiation pattern from the independent branches. The validity and efficiency of this proposed model are confirmed with a Fabry–Perot resonator antenna example.**

***Index Terms*— Artificial neural network (ANN), data classification, Fabry–Perot (FP) resonator antenna, performance parameters.**

I. Introduction

In recent years, a computer-aided design (CAD) approach based on artificial neural networks (ANNs) has been recognized as a powerful tool in electromagnetic (EM)-based modeling and design [1], [2], such as circuits [3]–[6], passive components [5], [7], [8], and field-effect transistors (FETs) [5], [8], [9]. Once the training process is completed, the trained ANN can be used in the place of EM simulations to significantly speed up EM-based modeling and design [10]. As improved approaches, the combination model of ANN and fuzzy inference system [11], ANN-based parametric frequency model [12], the combination model of ANN and FDTD [13], ANN-based Gaussian model [14], and ANN-based synthesis model [15] have been developed to improve the accuracy and reliability of antenna modeling and design. These models speed up model development and enhance the capability in learning.

An advanced modeling approach, which combines neural networks and transfer functions (neuro-TFs), is developed to perform parametric modeling of EM responses [16], [17]. This approach can be used even if accurate equivalent circuits or empirical models are unavailable. In [18], a technique is proposed to solve the discontinuity problem of neuro-TF. The model is verified with three parametric modeling examples, including a slotted patch antenna, a bandstop microstrip filter, and a bandpass coupled-line filter, through mapping the geometrical variables onto the S-parameter. An efficient neural-network method for EM behavior modeling of microwave filters with many input variables is proposed in [19]. Based on the decomposition approach to simply the high-dimensional problem into a set of low-dimensional ones, the validity of the model is confirmed with an H-plane filter and a side-coupled filter. In the modeling process of the neuro-TF model, the corresponding EM responses will lead to different orders of TFs when the number of the geometrical variations is large. The order-changing problem seriously deteriorates the convergence and accuracy of ANN. One common way to solve this problem is to set all TF orders to the maximum one among all geometrical samples. Recently, the pole/residue tracking technique has been proposed as another way to solve the order-changing problem for junction, filter, and antenna modeling [20].

Due to the limit of the reported neuro-TF model structure, only one performance parameter could be obtained from the output when geometrical variables are input. For antenna design, the operating frequency, bandwidth, gain, radiation pattern, and so on should be considered simultaneously. The result of a single S-parameter from neuro-TF models is insufficient to describe antenna performance.

To solve the issue of parametric modeling of antennas with multiparameters, an ANN model with a new structure is proposed to analyze a Fabry–Perot (FP) resonator antenna in this communication. Our model consists of three parallel branches which could simultaneously output the accurate results of S-parameter, gain, and radiation pattern. Each branch works independently in the training and testing processes. At the same time, the order-changing problem is solved from a new angle. The technique of data classification is incorporated into the proposed model to reduce the internal interference from the samples with different orders. This technique classifies the inputs during the training and testing processes. To make ANN accurately learn the mapping from geometrical variables to TF coefficients, the original training samples are classified into different categories according to TF orders. Here, the support vector machine (SVM) is trained with the collected geometrical variables and the corresponding TF orders in the training process, and then it classifies the geometrical variables into the proper categories in the testing process. The major advantage of SVM is the use of convex quadratic programing, which provides only global minima and avoids being trapped in local minima. Due to its advantageous nature, SVM has been applied to a wide range of classification tasks [21]–[24]. Thus, compared with neuro-TF models which only have a single S-parameter as output, the proposed model can output S-parameter, gain, and radiation pattern simultaneously for antenna simulation and design. Meanwhile, with data classification technique, the order-changing problem is solved from a new angle. Some multiobjective optimization algorithms, such as the nondominated sorting genetic algorithm II (NSGA-II) [25], multiobjective particle swarm optimization algorithm [26], [27], multiobjective genetic algorithm [28], and ε-constraint multiobjective optimization [29], have been employed for antenna optimization. As a typical multiobjective optimization algorithm, NSGA-II is selected to realize the optimization design of the FP resonator antenna in this communication.

II. Proposed Model

A. Whole Process of the Proposed ANN Model

The whole process of the proposed ANN model (as shown in Fig. 1) consists of the training process and the testing process.

In the training process, the training data are first obtained with the vector fitting technique which extracts the coefficients (or poles/residues) of TF from EM responses. Then in each branch

Manuscript received July 26, 2017; revised November 23, 2017; accepted March 30, 2018. Date of publication April 6, 2018; date of current version July 3, 2018. This work was supported in part by the National Natural Science Foundation of China under Grant 61471105 and Grant 61331007 and in part by 973 Project under Grant 613273. *(Corresponding author: Wei Shao.)*

The authors are with the School of Physics, University of Electronic Science and Technology of China, Chengdu 610054, China (e-mail: liyexiao@std.uestc.edu.cn; weishao@uestc.edu.cn; jinfulong_uestc@163.com; bzwang@uestc.edu.cn).

Color versions of one or more of the figures in this communication are available online at http://ieeexplore.ieee.org.

Digital Object Identifier 10.1109/TAP.2018.2823775

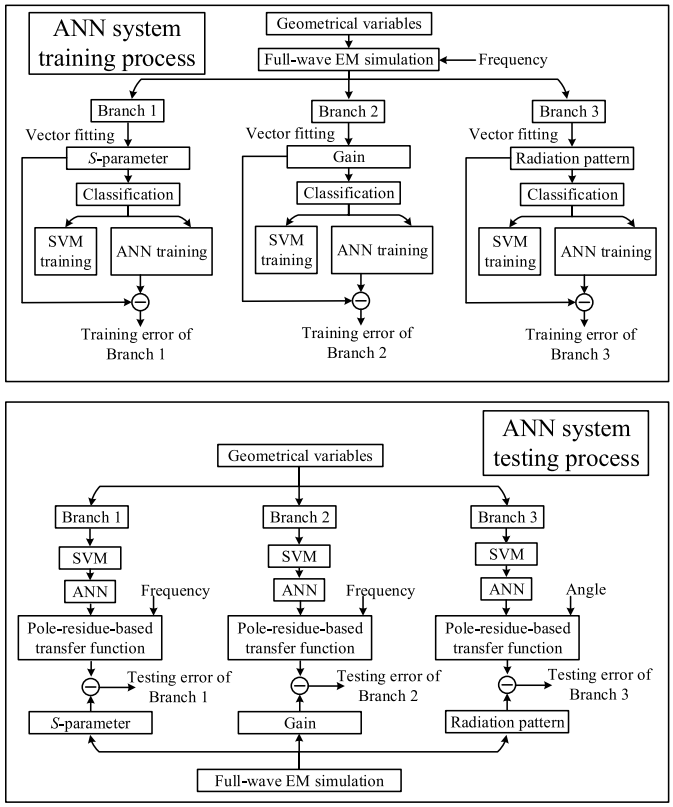

Fig. 1. Whole process of the ANN model.

which represents a certain antenna performance parameter, the original training data are classified into several categories for ANN and SVM training based on the TF orders to reduce the internal interference. The training data in each category are used to train the corresponding ANN to learn the nonlinear mapping between the geometrical variables and the coefficients of TF. Meanwhile, SVM is trained to learn the relationship between geometrical variables and the order of TF in each branch.

In the testing process, the geometrical variables are first input into the trained SVM and a matched category can be obtained. Then the geometrical variables are input into the corresponding ANN to output the pole and residue coefficients of TF.

B. Training Process of Branch 1

The structure of Branch 1 for S-parameter is shown in Fig. 2. To accurately map the relationship between geometrical variables and S-parameter with different TF orders, several ANNs are contained in this branch. $\boldsymbol{x}$ is a vector of the geometrical variables, representing the inputs of Branch 1, and the TF coefficients of S-parameter are set as outputs of ANNs. The pole-residue-based TF, an effective TF form used in EM simulations [20], is chosen in this communication. It is presented as

$$H(s) = \sum_{i=1}^{Q} \frac{r_i}{s - p_i} \tag{1}$$

where p_i and r_i are the pole and residue coefficients of TF, respectively, and Q is the order of TF.

The initial training data of neural networks are obtained with the vector fitting technique [30]. With vector fitting, we obtain the poles and residues of the transfer function corresponding to a given set of S-parameters. However, different S-parameter curves may lead to different TF orders. It is hard for the chaotic TF orders

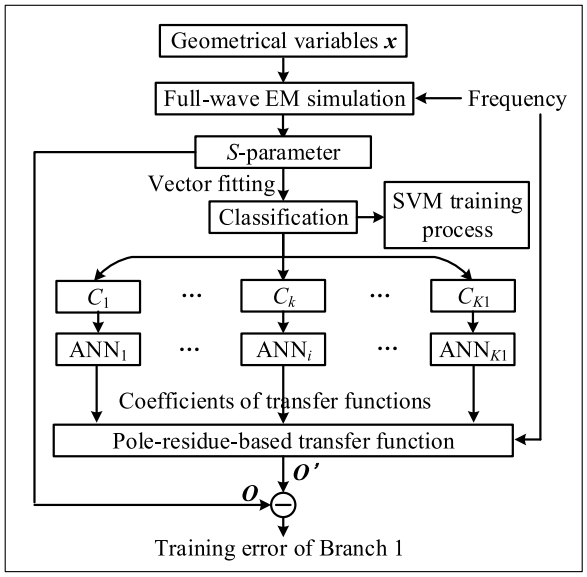

Fig. 2. Training process of Branch 1.

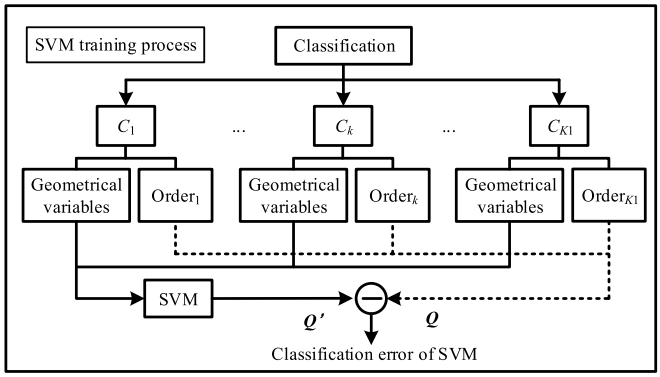

Fig. 3. Training process of SVM.

to train ANN accurately. Thus, according to the orders of TF, the original training samples are classified into different categories of C_k, $(k = 1, 2, \ldots, K1)$, where $K1$ is the total number of categories in Branch 1. The samples with the same TF order are classified into a category, and the order of each category could be presented as Q_k $(k = 1, 2, \ldots, K1)$.

Since the relationship between the poles/residues and $\boldsymbol{x}$ is nonlinear and unknown, ANNs are employed to learn this nonlinear relationship through the training process. Let $\boldsymbol{O} = \{O_1, K, O_W\}$ be a vector representing the outputs of the EM simulations (i.e., real and imaginary parts of S-parameters), where W is the number of the sample points of frequency. Let $\boldsymbol{O}' = \{O'_1, K, O'_W\}$ be a vector representing real and imaginary parts of the outputs of the pole-residue-based transfer function. The objective here is to minimize the error between $\boldsymbol{O}$ and $\boldsymbol{O}'$ for different $\boldsymbol{x}$ values, by adjusting the internal weights and thresholds of ANN. It is worth noting that one category is only used to train one ANN model named as ANN_k, $(k = 1, 2, \ldots, K1)$.

At the same time, the training samples are also used to train an SVM model, which determines the TF orders of $\boldsymbol{x}$ for classification during the testing process, as shown in Fig. 3. $\boldsymbol{x}$ is the input of SVM. Let $\boldsymbol{Q}' = \{Q'_1, K, Q'_{K1}\}$ be a vector representing the output of SVM, and $\boldsymbol{Q} = \{Q_1, K, Q_{K1}\}$ be a vector representing the actual order of TF. The training objective is to minimize the error between $\boldsymbol{Q}'$ and $\boldsymbol{Q}$ for different $\boldsymbol{x}$ values by adjusting the internal weights and

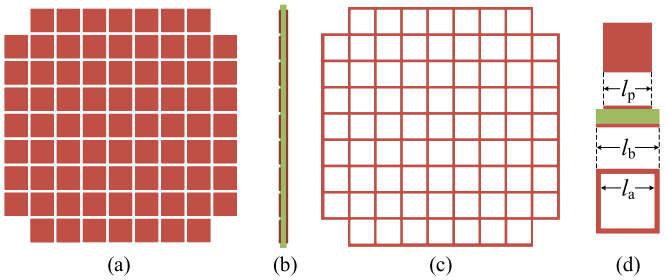

Fig. 4. EBG structure of the FP resonator antenna. (a) Top view. (b) Side view. (c) Bottom view. (d) Unit cell.

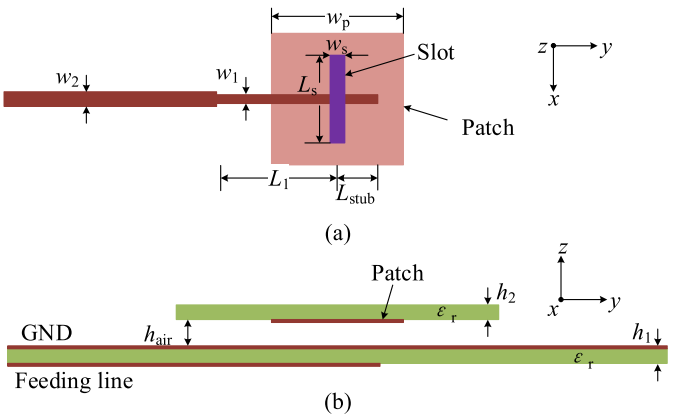

Fig. 5. Structure of the feeding antenna. (a) Top view. (b) Side view.

thresholds of SVM. For more details, one can refer to [31], which provides a complete description of the SVM theory.

The structure of Branch 2 for gain is similar to that of Branch 1. In Branch 3, the frequency in TF is replaced by the angle for the radiation pattern.

III. Application Example

The FP resonator antenna is a kind of highly directive antenna [32], which is formed by placing an EM bandgap (EBG) structure as a partially reflective surface (PRS) in front of a simple primary radiator with a ground plane. Its main advantages include high radiation efficiency and low complexity compared with the conventional antennas [33].

In this section, an FP resonator antenna proposed in [34] is considered as an example to evaluate the proposed ANN model. The EBG structure of this antenna, as shown in Fig. 4, is a combination of two complementary frequency selective surface (FSS) structures (square patches and square apertures). The EBG structure with a dimension of 72 mm × 72 mm ($2.4\lambda \times 2.4\lambda$ at 10 GHz) and 77 unit cells is arranged and applied as the PRS to the design of the FP resonator antenna. At each corner of the 9×9 rectangular array, one unit cell is eliminated. The metal patches and the square apertures are fabricated on the top and at the bottom of the substrate with a thickness of T and a relative dielectric constant of ε_r, respectively. The dimension ($l_b \times l_b$) of the unit cell is 8 mm × 8 mm (less than $\lambda/3$ at 10 GHz). l_p and l_a are the dimensions of the patch and aperture, respectively. The lateral dimension of the antenna is of the same size as the EBG structure.

The feeding structure which is an integral part of the FP resonator antenna is shown in Fig. 5. The parasitic patch is designed on the Rogers RT/duroid 5880 substrate ($\varepsilon_r = 2.2$ and $\tan\delta = 0.0009$). The feeding antenna is spaced from the ground plane by an air gap and

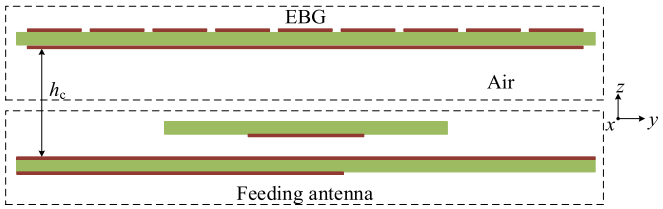

Fig. 6. Structure of the FP resonator antenna.

TABLE I
Definition of Training and Testing Data for the FP Resonator Antenna

Geometrical variables		Training data (64 samples)			Testing data (36 samples)		
		Min	Max	Step	Min	Max	Step
Case 1	l_p (mm)	5.6	6.3	0.1	5.65	6.15	0.1
	l_a (mm)	5.2	5.9	0.1	5.25	5.75	0.1
	h_c (mm)	14.5	15.55	0.15	14.575	15.325	0.15
Case 2	l_p (mm)	5.4	6.45	0.15	5.475	6.225	0.15
	l_a (mm)	5	6.05	0.15	5.075	5.825	0.15
	h_c (mm)	14.25	16	0.25	14.375	15.625	0.25

it is coupled with the feed line through a slot in the ground plane. The parameters of the antenna are as follows: $w_p = 9.3$ mm, $w_1 = 1.2$ mm, $w_2 = 2.3$ mm, $w_s = 2.3$ mm, $L_1 = 9.5$ mm, $L_s = 8.2$ mm, $L_{\text{stub}} = 3$ mm, $h_{\text{air}} = 2.5$ mm, and $h_1 = h_2 = 0.787$ mm.

Fig. 6 shows the whole structure of the FP resonator antenna. The feeding antenna is placed at the center of the cavity. h_c is the cavity height between the EBG layer and the ground plane.

Three geometrical variables of the EBG structure, i.e., $\boldsymbol{x} = [l_p \cdot l_a \cdot h_c]^T$, which play important roles in the performance of the antenna, are set as the input variables of the whole model.

The proposed model is applied to two different cases, i.e., Case 1 with a narrow parameter range and Case 2 with a wide one. In both cases, the training and testing data from the design of experiment method with eight levels (64 training samples) and six levels (36 testing samples) are shown in Table I, where the values of h_c are set around $\lambda/2$ and the values of l_p and l_a are set around $\lambda/5$ at 10 GHz [34]. The total time for training-data generation from EM simulations is 21.33 h, and the total time for testing-data generation is 12 h. Meanwhile, we use Hecht–Nelson method [35] to determine the node number of the hidden layer: the node number of the hidden layer is $2n + 1$ when the node number of the input layer is n.

HFSS 15.0 software performs the full-wave EM simulation and generates the training and testing data for modeling. All calculations in this communication are performed on an Intel i7-4870 2.50 GHz machine with 16 GB RAM.

A. S-Parameter

In Branch 1, the TF order of S-parameter varies slightly from 8 to 10 among the samples of different geometrical variables in Case 1. In Case 2, the TF order varies from 8 to 12. The training samples are divided into proper categories according to their TF orders for ANN training.

Meanwhile, the geometrical variables and corresponding TF orders from training samples are set as the input and output of SVM for training, respectively. For 36 testing samples, the classifying results are shown in Fig. 7. The classification precision of the trained SVM is 97.22%.

The mean absolute percentage error (MAPE) is used for performance evaluation and comparison in this communication

$$\text{MAPE} = \frac{1}{N}\sum_{n=1}^{N}\left|\frac{y_n - \hat{y}_n}{y_n}\right| \times 100\% \tag{2}$$

TABLE II

MODELING RESULTS OF THE PROPOSED MODEL FOR THE FP RESONATOR ANTENNA

S-parameter	Average training MAPE	Average testing MAPE
Case 1	0.399%	0.615%
Case 2	0.424%	0.672%
Gain	Average training MAPE	Average testing MAPE
Case 1	0.873%	0.954%
Case 2	0.857%	0.971%
Radiation pattern (E-plane)	Average training MAPE	Average testing MAPE
Case 1	2.645%	2.964%
Case 2	2.448%	2.912%
Radiation pattern (H-plane)	Average training MAPE	Average testing MAPE
Case 1	2.662%	2.973%
Case 2	2.441%	2.933%

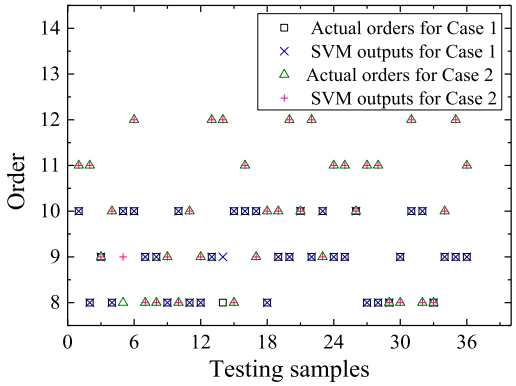

Fig. 7. Classifying results of S-parameter from SVM for Case 1 and Case 2.

where y_n and $\hat{y}_n$ denote the observed and forecasted values, respectively, of the nth datum, and N is the total number of the data. After the modeling process, the average training MAPEs of Branch 1 are 0.399% for Case 1 and 0.424% for Case 2, while the average testing MAPEs are 0.615% and 0.672%.

B. Gain

In Branch 2, the TF coefficients from a given set of broad-side radiation gain (z-direction in Fig. 6) of the FP resonator antenna are set as the outputs of ANNs. After the modeling process, the average training MAPEs of gain are 0.873% for Case 1 and 0.857% for Case 2, while the average testing MAPEs of gain are 0.954% and 0.971%.

C. Radiation Pattern

In Branch 3, ANNs are used for mapping the geometrical variables onto the TF coefficients which are extracted from two given sets of radiation patterns of the E-plane and H-plane at 10 GHz, respectively. Different from the above two branches, the angle in TF replaces the frequency, with an original range of $[-2\pi, 2\pi]$ for radiation pattern in this branch.

After the modeling process, the average training MAPEs are 2.645% for Case 1 and 2.448% for Case 2, while the average testing MAPEs are 2.964% and 2.912%. Due to the uneven curve of the radiation pattern, the training and testing MAPEs are higher than those in Branches 1 and 2. The whole modeling results of the proposed model are shown in Table II.

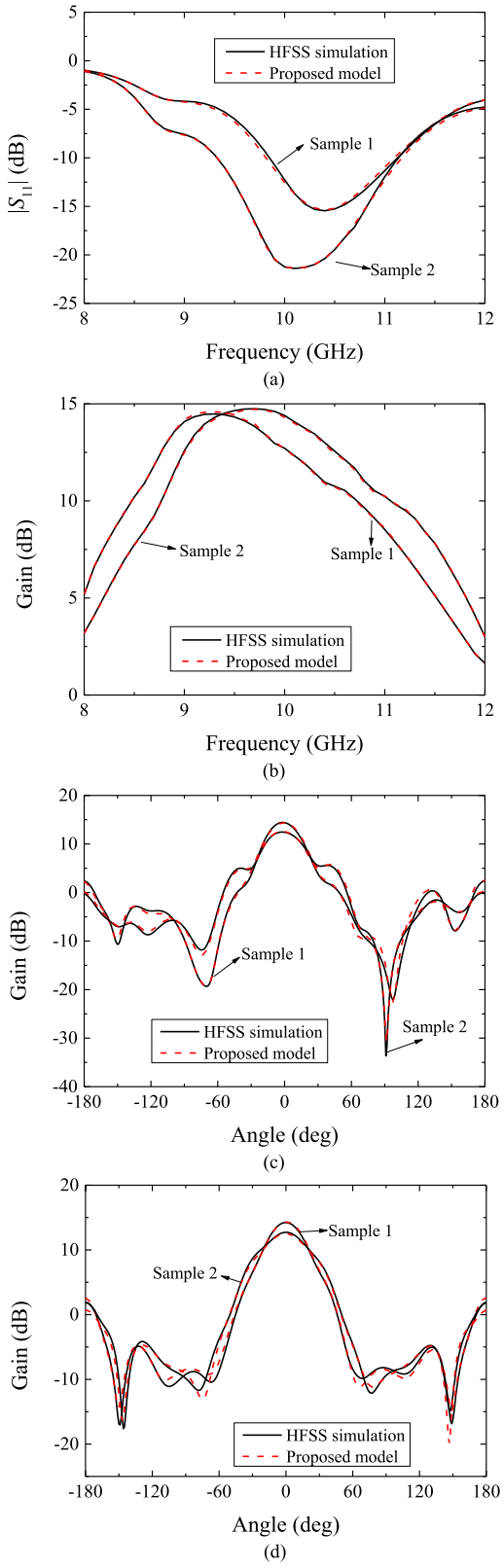

Fig. 8. Comparison between the proposed model and HFSS for samples 1 and 2. (a) S_{11}. (b) Gain. (c) E-plane pattern at 10 GHz. (d) H-plane pattern at 10 GHz, where the samples are in the range of training data.

D. Comprehensive Test

Fig. 8 shows the outputs of two different test geometrical samples of the FP resonator antenna with the proposed model and HFSS simulation. The variables for the two samples in the range of the training

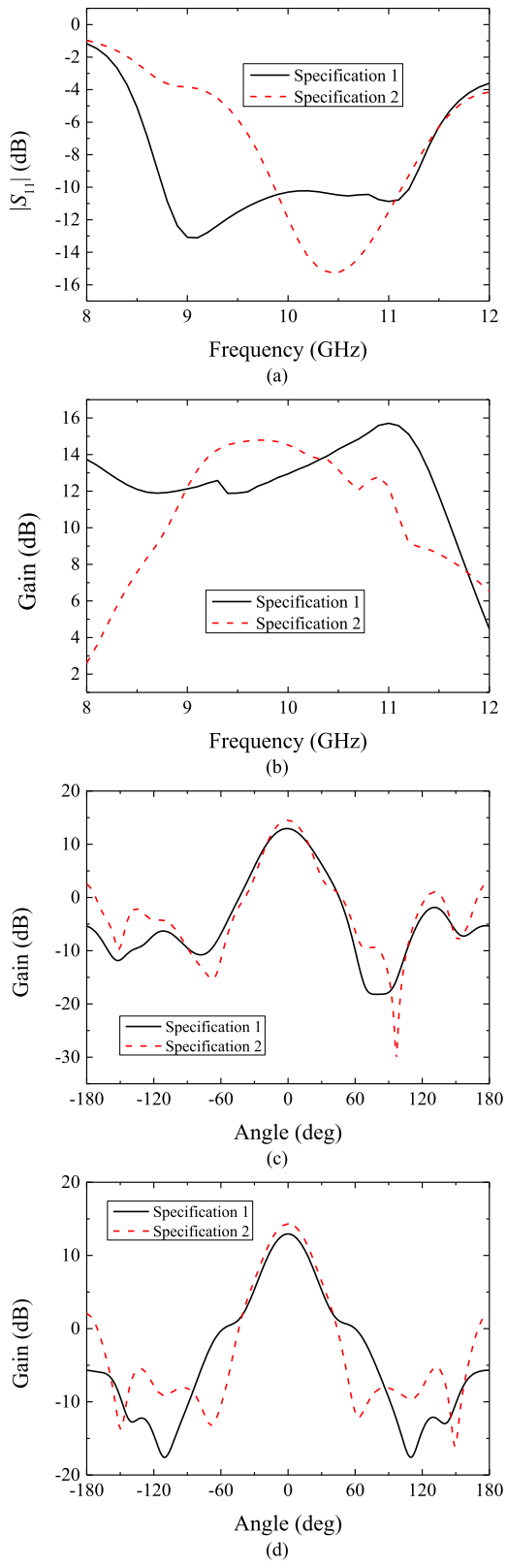

Fig. 9. Optimization results of specifications 1 and 2 from the trained model. (a) S_{11} parameter. (b) Gain. (c) E-plane pattern at 10 GHz. (d) H-plane pattern at 10 GHz.

data are $\boldsymbol{x}_1 = [5.62 \cdot 5.44 \cdot 14.63]^T$ and $\boldsymbol{x}_2 = [5.87 \cdot 5.51 \cdot 15.36]^T$. The average MAPEs of S-parameter for the two samples are 0.605% and 0.569%. The average MAPEs of gain for the two samples are 0.964% and 0.969%. The average MAPEs of the E-plane pattern for the two samples are 2.936% and 2.954%, and average MAPEs are 2.934% and 2.951% for the H-plane pattern. It is observed that the proposed model can achieve good accuracy when the geometrical samples are never used in training.

TABLE III
RUNNING TIME OF DIRECT EM OPTIMIZATION AND THE PROPOSED MODEL

	CPU time of model development	
	Direct EM optimization	Proposed model
Antenna 1	45 hours	60 s
Antenna 2	49 hours	60 s
Total	94 hours	33.33 hours (modeling) + 120 s

Two other test geometrical samples, which are selected out of the range of the training data, are chosen to evaluate the proposed model. The variables for the two samples are $\boldsymbol{x}_1' = [5.3 \cdot 4.9 \cdot 14.2]^T$ and $\boldsymbol{x}_2' = [6.5 \cdot 4.9 \cdot 16.1]^T$. The average MAPEs of S-parameter for the two samples are 0.553% and 0.515%. The average MAPEs of gain for the two samples are 0.959% and 0.961%. The average MAPEs of the E-plane pattern for the two samples are 2.913% and 2.947%, and average MAPEs 2.946% and 2.933% for the H-plane pattern. It is observed that our model can achieve good accuracy even though the geometrical samples are out of the range of the training data.

E. Application of Optimization

Once the training is completed, the trained model which is a substitute for the time-consuming EM simulation can be applied to the design optimization. As an example of using the trained model for antenna design, two separate FP resonator antennas are optimized to reach two different design specifications.

The following are the optimization objectives of specification 1:
1) $|S_{11}| \leq -10$ dB at the frequency range of 8.75–11.25 GHz;
2) relative 3 dB gain bandwidth reaches 32%;
3) gain of the main lobe $G_{\max} \geq 12.5$ dB.

The following are the optimization objectives of specification 2:
1) $|S_{11}| \leq -10$ dB at the frequency range of 10–11 GHz;
2) relative 3 dB gain bandwidth reaches 21%;
3) gain of the main lobe $G_{\max} \geq 14$ dB.

With NSGA-II, the optimization of the FP resonator antennas is performed by calling the trained model repeatedly. The initial variables are chosen as $\boldsymbol{x}_{\text{initial}} = [15 \cdot 5.5 \cdot 6]^T$. The optimization spends only about 60 s to achieve the optimal solution for each antenna, as shown in Fig. 9. The optimized geometrical values for the two separate antennas are $\boldsymbol{x}_{\text{opt1}} = [14.748 \cdot 5.189 \cdot 5.904]^T$ and $\boldsymbol{x}_{\text{opt2}} = [14.733 \cdot 6.011 \cdot 6.401]^T$ which are selected from the Pareto fronts.

Compared with the directive EM optimization in which the EM simulations are repeatedly called by NSGA-II, the design using the trained model could save considerable time, as shown in Table III.

IV. CONCLUSION

In this communication, a novel neuro-TF model is proposed to address the issue of multiparameter modeling of antennas. This model includes three parallel and independent branches. Once the geometrical variables are input, it can simultaneously obtain S-parameter, gain, and radiation pattern from the corresponding branch, respectively. Meanwhile, a data-classification technique of SVM is introduced to classify the geometrical variables into the proper categories in each branch. An FP resonator antenna is employed to validate this proposed model. The trained model provides its powerful computing ability especially in the field of EM optimization design.

REFERENCES

[1] P. Burrascano, S. Fiori, and M. Mongiardo, "A review of artificial neural networks applications in microwave computer-aided design," *Int. J. RF Microw. Comput.-Aided Eng.*, vol. 9, no. 3, pp. 158–174, May 1999.

[2] M. B. Steer, J. W. Bandler, and C. M. Snowden, "Computer-aided design of RF and microwave circuits and systems," *IEEE Trans. Microw. Theory Techn.*, vol. 50, no. 3, pp. 996–1005, Mar. 2002.

[3] J. E. Rayas-Sanchez, "EM-based optimization of microwave circuits using artificial neural networks: The state-of-the-art," *IEEE Trans. Microw. Theory Techn.*, vol. 52, no. 1, pp. 420–435, Jan. 2004.

[4] V. Rizzoli, A. Costanzo, D. Masotti, A. Lipparini, and F. Mastri, "Computer-aided optimization of nonlinear microwave circuits with the aid of electromagnetic simulation," *IEEE Trans. Microw. Theory Techn.*, vol. 52, no. 1, pp. 362–377, Jan. 2004.

[5] V. K. Devabhaktuni, C. Xi, F. Wang, and Q.-J. Zhang, "Robust training of microwave neural models," *Int. J. RF Microw Comput.-Aided Eng.*, vol. 12, no. 1, pp. 109–124, 2002.

[6] A. Veluswami, M. S. Nakhla, and Q.-J. Zhang, "The application of neural networks to EM-based simulation and optimization of interconnects in high-speed VLSI circuits," *IEEE Trans. Microw. Theory Techn.*, vol. 45, no. 5, pp. 712–723, May 1997.

[7] J. W. Bandler, M. A. Ismail, J. E. Rayas-Sánchez, and Q.-J. Zhang, "Neuromodeling of microwave circuits exploiting space-mapping technology," *IEEE Trans. Microw. Theory Techn.*, vol. 47, no. 12, pp. 2417–2427, Dec. 1999.

[8] V. K. Devabhaktuni, M. C. E. Yagoub, and Q.-J. Zhang, "A robust algorithm for automatic development of neural-network models for microwave applications," *IEEE Trans. Microw. Theory Techn.*, vol. 49, no. 12, pp. 2282–2291, Dec. 2001.

[9] F. Wang and Q.-J. Zhang, "Knowledge-based neural models for microwave design," *IEEE Trans. Microw. Theory Techn.*, vol. 45, no. 12, pp. 2333–2343, Dec. 1997.

[10] Q.-J. Zhang, K. C. Gupta, and V. K. Devabhaktuni, "Artificial neural networks for RF and microwave design—From theory to practice," *IEEE Trans. Microw. Theory Techn.*, vol. 51, no. 4, pp. 1339–1350, Apr. 2003.

[11] K. Guney and N. Sarikaya, "A hybrid method based on combining artificial neural network and fuzzy inference system for simultaneous computation of resonant frequencies of rectangular, circular, and triangular microstrip antennas," *IEEE Trans. Antennas Propag.*, vol. 55, no. 3, pp. 659–668, Mar. 2007.

[12] Y. Kim, S. Keely, J. Ghosh, and H. Ling, "Application of artificial neural networks to broadband antenna design based on a parametric frequency model," *IEEE Trans. Antennas Propag.*, vol. 55, no. 3, pp. 669–674, Mar. 2007.

[13] H. J. Delgado and M. H. Thursby, "A novel neural network combined with FDTD for the synthesis of a printed dipole antenna," *IEEE Trans. Antennas Propag.*, vol. 53, no. 7, pp. 2231–2236, Jul. 2005.

[14] K. C. Lee, "Application of neural network and its extension of derivative to scattering from a nonlinearly loaded antenna," *IEEE Trans. Antennas Propag.*, vol. 55, no. 3, pp. 990–993, Mar. 2007.

[15] T. Khan, A. De, and M. Uddin, "Prediction of slot-Size and inserted air-gap for improving the performance of rectangular microstrip antennas using artificial neural networks," *IEEE Antennas Wireless Propag. Lett.*, vol. 12, pp. 1367–1371, 2013.

[16] X. Ding *et al.*, "Neural-network approaches to electromagnetic-based modeling of passive components and their applications to high-frequency and high-speed nonlinear circuit optimization," *IEEE Trans. Microw. Theory Techn.*, vol. 52, no. 1, pp. 436–449, Jan. 2004.

[17] V. M.-R. Gongal-Reddy, F. Feng, and Q.-J. Zhang, "Parametric modeling of millimeter-wave passive components using combined neural networks and transfer functions," in *Proc. Global Symp. Millim. Waves (GSMM)*, Montreal, QC, Canada, May 2015, pp. 1–3.

[18] Y. Cao, G. Wang, and Q.-J. Zhang, "A new training approach for parametric modeling of microwave passive components using combined neural networks and transfer functions," *IEEE Trans. Microw. Theory Techn.*, vol. 57, no. 11, pp. 2727–2742, Nov. 2009.

[19] H. Kabir, Y. Wang, M. Yu, and Q.-J. Zhang, "High-dimensional neural-network technique and applications to microwave filter modeling," *IEEE Trans. Microw. Theory Techn.*, vol. 58, no. 1, pp. 145–156, Jan. 2010.

[20] F. Feng, C. Zhang, J. Ma, and Q.-J. Zhang, "Parametric modeling of EM behavior of microwave components using combined neural networks and pole-residue-based transfer functions," *IEEE Trans. Microw. Theory Techn.*, vol. 64, no. 1, pp. 60–77, Jan. 2016.

[21] C. Cortes and V. Vapnik, "Support-vector networks," *Mach. Learn.*, vol. 20, no. 3, pp. 273–297, 1995.

[22] K.-S. Shin, T. S. Lee, and H. Kim, "An application of support vector machines in bankruptcy prediction model," *Expert Syst. Appl.*, vol. 28, no. 1, pp. 127–135, 2005.

[23] H.-L. Chen, D.-Y. Liu, B. Yang, J. Liu, and G. Wang, "A new hybrid method based on local fisher discriminant analysis and support vector machines for hepatitis disease diagnosis," *Expert Syst. Appl.*, vol. 38, no. 9, pp. 11796–11803, 2011.

[24] H. L. Chen, B. Yang, J. Liu, and D.-Y. Liu, "A support vector machine classifier with rough set-based feature selection for breast cancer diagnosis," *Expert Syst. Appl.*, vol. 38, no. 7, pp. 9014–9022, 2011.

[25] K. Deb, A. Pratap, S. Agarwal, and T. Meyarivan, "A fast and elitist multiobjective genetic algorithm: NSGA-II," *IEEE Trans. Evol. Comput.*, vol. 6, no. 2, pp. 182–197, Apr. 2002.

[26] J. Lu, D. Ireland, and A. Lewis, "Multi-objective optimization in high frequency electromagnetics—An effective technique for smart mobile terminal antenna (SMTA) design," *IEEE Trans. Magn.*, vol. 45, no. 3, pp. 1072–1075, Mar. 2009.

[27] S. Chamaani, S. A. Mirtaheri, and M. S. Abrishamian, "Improvement of time and frequency domain performance of antipodal vivaldi antenna using multi-objective particle swarm optimization," *IEEE Trans. Antennas Propag.*, vol. 59, no. 5, pp. 1738–1742, May 2011.

[28] X. Yuan *et al.*, "A parasitic layer-based reconfigurable antenna design by multi-objective optimization," *IEEE Trans. Antennas Propag.*, vol. 60, no. 6, pp. 2690–2701, Jun. 2012.

[29] D. W. Boeringer and D. H. Werner, "Bezier representations for the multiobjective optimization of conformal array amplitude weights," *IEEE Trans. Antennas Propag.*, vol. 54, no. 7, pp. 1964–1970, Jul. 2016.

[30] B. Gustavsen and A. Semlyen, "Rational approximation of frequency domain responses by vector fitting," *IEEE Trans. Power Del.*, vol. 14, no. 3, pp. 1052–1061, Jul. 1999.

[31] N. Cristianini and J. Shawe-Taylor, *An Introduction to Support Vector Machines: and Other Kernel-Based Learning Methods*. Cambridge, U.K.: Cambridge Univ Press, 2000.

[32] A. P. Feresidis and J. C. Vardaxoglou, "High gain planar antenna using optimised partially reflective surfaces," *IEE Proc.-Microw., Antennas Propag.*, vol. 148, no. 6, pp. 345–350, Dec. 2001.

[33] A. R. Weily, K. P. Esselle, T. S. Bird, and B. C. Sanders, "High gain circularly polarised 1-D EBG resonator antenna," *Electron. Lett.*, vol. 42, no. 18, pp. 1012–1013, Aug. 2006.

[34] N. Wang, Q. Liu, C. Wu, L. Talbi, Q. Zeng, and J. Xu, "Wideband Fabry–Perot resonator antenna with two complementary FSS layers," *IEEE Trans. Antennas Propag.*, vol. 62, no. 5, pp. 2463–2471, May 2014.

[35] S. R. Hecht-Nielsen, "Kolmogorov's mapping neural network existence theorem," in *Proc. IEEE Joint Conf. Neural Netw.*, vol. 3. New York, NY, USA, 1987, pp. 11–14.